

An Interaction-Aware, Perceptual Model for Non-Linear Elastic Objects

Michal Piovarčí^{1,2} David I.W. Levin⁵ Jason Rebello⁶ Desai Chen⁴ Roman Ďuríkovič²
Hanspeter Pfister⁶ Wojciech Matusik⁴ Piotr Didyk^{1,3}

¹Saarland University, MMCI ²Comenius University ³MPI Informatik ⁴MIT CSAIL ⁵Disney Research ⁶Harvard University

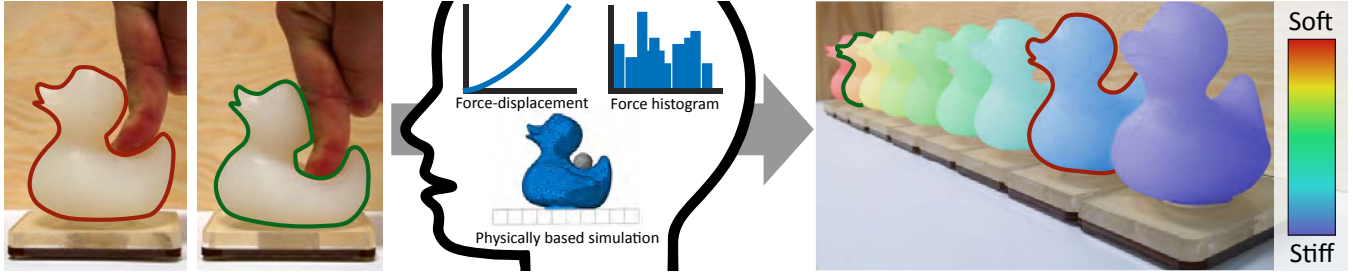


Figure 1: 3D printing allows us to print objects with varying deformation properties. The question that we want to answer is: Given a set of printing materials and a 3D object with desired elasticity properties, which material should be used to print the object? For example, given sample ducks (left) with desired elasticity properties (e.g., measured), our system considers several candidate materials that can be used for replicating the ducks (right), and chooses materials that will best match compliance properties when examined by an observer (red and green outlines). Moreover, we can sort all possible materials by their perceived compliance as predicted by our model. The measured compliance is indicated with colors ranging from stiff (blue) to soft (red).

Abstract

Everyone, from a shopper buying shoes to a doctor palpating a growth, uses their sense of touch to learn about the world. 3D printing is a powerful technology because it gives us the ability to control the haptic impression an object creates. This is critical for both replicating existing, real-world constructs and designing novel ones. However, each 3D printer has different capabilities and supports different materials, leaving us to ask: How can we best replicate a given haptic result on a particular output device? In this work, we address the problem of mapping a real-world material to its nearest 3D printable counterpart by constructing a perceptual model for the compliance of nonlinearly elastic objects. We begin by building a perceptual space from experimentally obtained user comparisons of twelve 3D-printed metamaterials. By comparing this space to a number of hypothetical computational models, we identify those that can be used to accurately and efficiently evaluate human-perceived differences in nonlinear stiffness. Furthermore, we demonstrate how such models can be applied to complex geometries in an interaction-aware way where the compliance is influenced not only by the material properties from which the object is made but also its geometry. We demonstrate several applications of our method in the context of fabrication and evaluate them in a series of user experiments.

Keywords: compliance, fabrication, perception, haptics

Concepts: •Computing methodologies → Perception; Physical simulation; •Human-centered computing → User studies;

1 Introduction

One of the benefits of 3D printing is that it allows us to control not just the appearance of an object, but also its haptic properties. This is of broad importance, from designing comfortable clothing to building medical phantoms for surgeons and doctors. Unfortunately, the material gamut of individual printing platforms is limited and, just as a 2D printer with a limited color gamut can introduce artifacts into an image, material limits can cause unintended changes in the haptic properties of a 3D printed design.

Minimizing these artifacts requires a method for optimally projecting a design onto the material space of a given printer, and this projection requires a suitable metric. Currently, people use standard metrics to quantify differences in material mechanical properties. The typical approach is comparing L2 norms of stress-strain curves [Bickel et al. 2010]. However, such metrics ignore a major component of haptic interaction, the users themselves. Previous work which explores similar problems for visual output devices has found that perceptual metrics can outperform standard measures [Morovic and Luo 2001; Reinhard et al. 2010]. In this work we seek to find a computationally efficient and accurate perceptual model for compliance of 3D printed objects that will allow us to compare them in a meaningful way.

Newer 3D printers, such as the Objet500 Connex Series from Stratasys, are not limited to printing rigid materials. Previous work [Bickel et al. 2010; Schumacher et al. 2015; Panetta et al. 2015] has demonstrated that, by varying the internal structure of an object, so-called metamaterials can be created. These metamaterials increase the gamut of printable, non-linearly elastic materials available. Correspondingly, we do not limit our investigations to rigid or linearly elastic materials but instead develop a metric suitable for nonlinearly elastic materials for which the internal forces are an arbitrary function of the applied deformation.

In order to design a suitable metric for comparing compliance of different materials, as perceived by a human, we first compute a perceptual space – a space wherein the Euclidean distances between samples correspond to magnitudes of perceived differences. Inspired

by [Pellacini et al. 2000; Wills et al. 2009], we construct a pointwise approximation by applying multi-dimensional scaling to a predefined set of compliant 3D printed metamaterials. This, however, does not provide us with a closed-form transformation between different materials and the perceptual space, which is desired for many applications. Therefore, we evaluate a number of candidate computational models, and propose one that provides a mapping that best describes the empirical data. While the psychophysical experiments for evaluating the models are performed on simple-shape stimuli, we also demonstrate how to apply our model to complex geometries such that it accounts for geometrical variations in designs. Finally, we present several applications of our model in the context of 3D printing. To summarize, our contributions are:

- a psychophysical experiment evaluating compliance of different metamaterials produced using a 3D printer together with a corresponding perceptual space,
- new computational models for perceived compliance that incorporate force information,
- evaluation of these and previously proposed models based on our empirical experiment,
- an extension of the model derived for a simple shape to complex geometries,
- several examples of applying the model for 3D printing complex objects with different compliance properties, and
- a validation of our results in a series of user experiments.

2 Related Work

Studies on material perception have been primarily concerned with understanding two categories of object properties – visual and haptic. We begin by exploring previous work on compliance perception and continue by reviewing work on perception of visual properties, with a focus on the recent work from the computer graphics community.

2.1 Compliance Perception

Compliance describes how a given material reacts when a force is applied. In the case of linearly elastic materials, compliance is defined as an inverse of stiffness – the ratio of material deformation to applied force. By definition, for linear materials, this ratio is constant. In the context of nonlinear materials, the relationship between force and displacement is nonlinear and therefore stiffness can be defined only locally, as the tangent to the force-displacement curve. In this paper we use the term stiffness to refer to this local material tangent and the term compliance (the inverse of stiffness) to refer to the mechanical behavior of an entire object.

Factors and Cues Compliance perception is a complex phenomenon and many different cues are used by humans to judge material softness. They range from purely kinesthetic, e.g., applied force, displacement, pressure distribution, surface deformation [Friedman et al. 2008; Tiest and Kappers 2009], to visual [Kuschel et al. 2010; Wu et al. 1999]. As a result, many factors affect perceived compliance. For example, it has been demonstrated that softness perception can vary depending on the mode of interaction or velocity with which the stimuli is compressed [Friedman et al. 2008]. Even such things as texture, sample size, and location can influence the perceived compliance [Wu et al. 1999]. Moreover, compliance perception is closely related to cutaneous tactile information such as fingerpad contact area spread rate [Ambrosi et al. 1999]. For a great overview of mechanisms behind more general haptic perception, please refer to [Lederman and Klatzky 2009]. In this work, we are concerned only with the kinesthetic cues, i.e., the computational models that we consider in this paper do not account

for any visual cues – we prevent any visual inspection of tested samples in the psychophysical experiments which were used to build our model.

Compliance Discrimination Human ability to discriminate between linear materials of varying stiffness has been extensively studied and it has been shown that compliance perception obeys Weber's law, i.e., the ratio between the smallest compliance difference that can be detected and the compliance of the stimuli is constant and equal to the so-called Weber fraction. For example, Tan et al. [1992] showed that (using a vernier caliper) the Weber fraction is 8% when the displacement applied to the object is fixed and 22% when the displacement is allowed to vary. These experiments corroborate those of Jones et al. [1990], who reported that the Weber fraction is stable from 670 N/m to 6260 N/m, and equal to approximately 23%. Compliance discrimination can also be greatly affected by lack of certain cues. For example, lack of a work cue and minimized force cue can increase the Weber fraction to 99% [Tan et al. 1993], which suggests that these cues might be crucial for discriminating between the softness of different materials. Interestingly, it has been demonstrated that the Weber fraction for compliance is much higher than for force and displacement [Jones and Hunter 1990]. Koçak et al. [2011] reported that there is also a memory influence on compliance discrimination. Their experiments, performed using a haptic device, found that participants are more sensitive to softness changes during continuous presentation, i.e., when investigation of one sample is followed directly by another sample. More recently, Weber fraction has been also measured for a haptic jamming display to be 16% [Genecov et al. 2014].

Difference Magnitudes Estimations Studies on compliance discrimination give us insights into human ability to detect different levels of softness. To better understand the characteristics of perceived compliance, it is necessary to estimate the magnitude of perceived differences. One such experiment was conducted by Harper et al. [1964]. They tested subjective hardness of nine compliant specimens and calculated the relationship to physical stiffness. Magnitude estimation tests were also performed more recently by Friedman et al. [2008]. In that work, the main goal was to investigate how different modes of interaction affect the compliance perception.

Perceptual Space of Compliance Magnitudes of perceived differences can be further used to compute a perceptual space. A common technique used for this purpose is multi-dimensional scaling (MDS). It takes, as input, pair-wise distances between stimuli and computes an embedding of all samples in a multi-dimensional space which respects their relative positions. When the input distances are obtained using a psychophysical experiment, in which people judge differences between stimuli, the perceived differences between samples can be approximated as Euclidian distances in the computed space. MDS has been previously applied to investigate different aspects of haptic perception. For example, Bergmann et al. [2006] analyzed compressibility and roughness of 124 different material samples and found a four-dimensional space to be sufficient to describe the space of all samples. Similar experiments were performed by Hollins et al. [2000]. More recently, MDS was used by Cooke et al. [2006; 2010] to investigate shape and texture perception of rigid objects. The experiments most similar to ours are [Leškowský et al. 2006; Misra et al. 2009]. Leškowský et al. [2006] used MDS to investigate the difference between real and virtual compliant objects. They found that a one-dimensional space is sufficient to describe real samples, which agrees with our findings. However, when virtual samples are added, two dimensions are required. Misra et al. [2009] used MDS to quantify the role of the Poynting effect (i.e., a presence of normal forces during shearing) on material perception.

Computational Models for Compliance Several computational models for perceived compliance have been proposed in the context of haptic telemanipulation systems. Pressman et al. [2007] found that delay between force and displacement can significantly affect the softness perceived by an operator. To predict the modified perception they investigated several computational models and showed that some of them, e.g., peak-force to displacement ratio, local stiffness, and maximum force can predict the phenomenon well. Later work [Pressman et al. 2011] showed that these models are powerful predictors of the perceptual effect on a compliance sensation induced when the position of an object is changed without visual feedback. These models were tested on linearly elastic materials, but delay added to haptic interaction introduced velocity-dependent, non-linear behavior. Leib et al. [2010] considered a similar situation, but this time the relationship between position and force was pairwise linear and independent of velocity. In their work, an additional computational model was considered in which compliance was estimated as the inverse of the slope of a line fitted to the force-displacement curve. Subsequent work by [Nisky et al. 2011] considered the effect of a delay in the context of the nonlinear behavior of a haptic device.

In our experiments, instead of estimating Weber fraction or discrimination thresholds, we focus on measuring perceived distances between materials and objects with different nonlinear stiffnesses. Therefore, our psychophysical experiments are similar to magnitude estimation studies. In our work, however, the perceived distances are estimated indirectly using a non-metric MDS which provides more robust estimates [Wills et al. 2009] than the standard variant. Our construction of a perceptual space is similar to previous work that investigates compliance based on MDS results, but it is different in that we consider highly nonlinear materials and build a computational model that predicts perceived compliance differences. This is also different from previous work on computational models for compliance which aim at predicting detection thresholds. However, the models evaluated here are inspired by this line of work. One of the major differences in our study is that prior experiments were performed in laboratory conditions using specialized equipment while we consider a scenario which is tailored towards 3D printing applications. We also eschew haptic devices, instead performing experiments using real-world materials.

2.2 Material Perception in Computer Graphics

In computer graphics, the perceptual study of materials has mostly focused on their visual properties. In this context, our work is similar to Pellacini et al. [2000] and Wills et al. [2009], which propose a perceptual space for gloss, and Gkioulekas et al. [2013], where perception of translucent materials is studied. Pellacini et al. use standard multi-dimensional scaling (MDS), which is based on the distances between different images reported by a subject, to learn a two-dimensional space of bi-direction reflectance distribution functions (BRDF). Wills et al. use a non-metric multi-dimensional scaling (NMDS) to build a similar space but for a larger range of BRDFs. In contrast to MDS, NMDS does not require the magnitude of the dissimilarities between BRDFs, but only their ordering. This helps in reducing the inter- and intra-subject variance observed in user studies. In their work on transparency perception, Gkioulekas et al. [2013] use both MDS (to build a space of translucent materials based on an image metric) and NMDS (to obtain a similar space from user data). Like these works we also build a perceptual space of compliance using non-metric MDS in order to analyze our collection of computational models. Recently, also auditory perception of different materials has been investigated to improve sound rendering techniques [Ren et al. 2013]. Han and Keyser [2015] examined the influence of material appearance on the deformation perception and demonstrated that appearance can influence the judgment of softness. In the context of fabrication, Zhang et al. [2015] proposed

a method for optimizing printing direction that minimizes visual artifacts in printed objects. Our work contributes to these efforts in improving fabrication techniques by incorporating knowledge about perception.

3 Overview

The goal of this work is to relate the physical compliance of an object to its perceived compliance when examined by a human. Since physical stiffness can be expressed using measured force-displacement data, we consider this as the main cue for compliance. Consequently, we seek a relation between the force-displacement characteristic and the "feeling" of compliance. To determine this relationship we first perform a psychophysical experiment with simple 3D-printed stimuli (small cubes), for which we can easily vary the force-displacement characteristic (Section 4). Based on the perceptual space of the stimuli derived using non-metric multi-dimensional scaling, we evaluate various computational models that predict perceived compliance from the force-displacement characteristic (Section 5). Once a suitable one-dimensional relationship has been identified, we show how numerical simulation can be used to extend the model to complex geometries with which users interact via poking (Section 6). To do this we exploit the fact that applying a virtual point load to a simulated object yields a local, 1D, force-displacement curve, to which the computational model is applied. As a result, a spatially-varying map of the perceived compliance is obtained. Finally, we present several applications of our perceptual model in the context of 3D printing and rapid prototyping (Section 7).

4 Perceptual Space of Stiffness

Our perceptual compliance space is computed using non-metric multi-dimensional scaling [Wills et al. 2009] using data of paired comparisons between samples. Below we describe, in detail, the stimuli, experiment, and the analysis used for deriving the space.

4.1 Stimuli

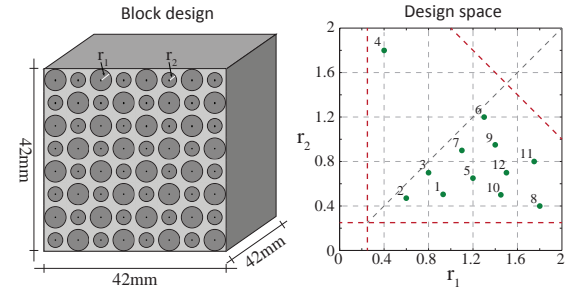


Figure 3: Left: Design of our samples. Equally spaced out cylindrical holes are defined using two radii. Right: Parameter of our samples. The two axes correspond to two radii of the cylinders (in mm). 12 green dots correspond to the samples used for our experiment. The red lines indicate the lower limits for the values of the radii, due to the printer resolution, and the upper limit for radii to guarantee that the cylinders do not intersect. Block 4 was introduced as a counterpart of block 8 to verify whether compliance properties are symmetric with respect to the choice of radii.

Current 3D printers use a relatively small number of printing materials, which restricts the spectrum of deformation properties that can be produced. Our experiment requires material samples with diverse mechanical properties. To counteract the limitation of 3D prints, we fabricate metamaterials with different internal structures. As presented in Figure 3 (left), our samples were designed as cubes

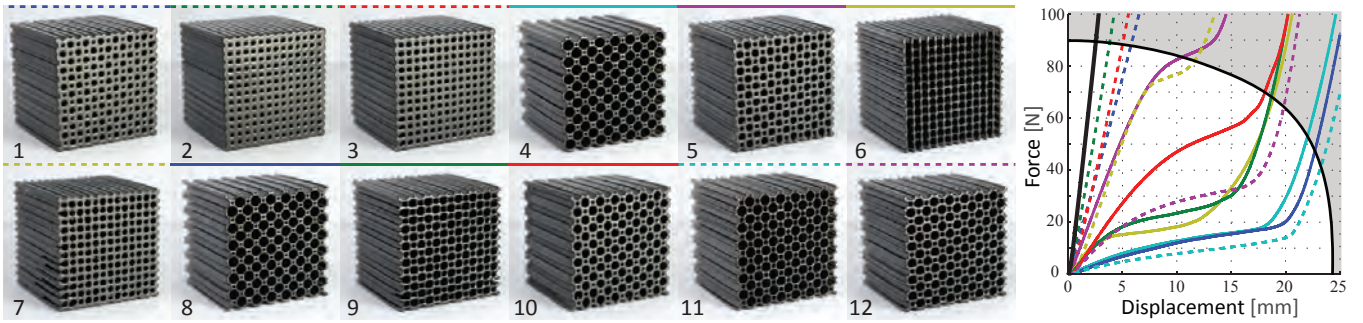


Figure 2: The 12 stimuli that were used in our experiments. The plot on the right shows corresponding force-displacement curves obtained via uniaxial test. The lines above blocks indicate the corresponding line styles. For a reference, we also include the force-displacement curve for a solid block (black line). The gray area roughly marks maximum applied force to each sample. For exact values please refer to the supplementary material.

with cylindrical holes of two sizes, spaced regularly across the sample. Each sample was defined by 4 parameters: block size, distance between centers of the cylinders, and two radii for the cylinders. For our experiment, we limited the design space to 42 mm blocks where centers of circles were kept at a constant distance of 3 mm. Different stiffness was achieved by varying the two radii parameters, which were kept between 0.5 mm and 2 mm due to manufacturing limitations. After accounting for the fact that the cylinders cannot intersect, we sampled our design space uniformly (Figure 3, right). We designed 12 different blocks in total, and printed them using TangoBlack+ material on a Stratasys Objet500 3D printer. Similar, foam-like metamaterials were used by Bickel et al. [2010] for printing objects with desired deformation properties.

To characterize the material properties of each block, we perform uniaxial load testing. An increasing force (up to 100 N) was applied to each block at constant speed of 0.1 mm/s, and the corresponding deformation was recorded. Figure 2 shows all the samples used in the experiment along with their corresponding force-displacement curves.

4.2 Methodology

During each trial of our experiment, participants were presented with one reference block and two test blocks arranged in a row. They were asked to judge which test block was more similar to the reference in terms of softness. Participants were asked to interact with the samples in a direction perpendicular to their surface. This interaction mode removes the effect of anisotropy present in the fabricated cubes. No limitations on the number of interactions during a single trial were imposed. Visual feedback was avoided by placing all blocks under a cover. The experimental setup is presented in Figure 4. The 12 blocks considered in our experiment resulted in 660 different possible trial combinations. The study was performed by 20 subjects. Each subject was presented with 78 trials which resulted in a total of 1,560 comparisons. The average duration of the experiment was about one hour. Participants were allowed to take a break halfway through the experiment.

4.3 Data Reliability

We evaluated the quality of our data using three additional experiments. First, we evaluated the intra-subject consistency. We presented a random set of 9 triples, 4 times each to every participant. On average, in 72.22% of the cases subjects gave the same answer. Next, to test the inter-subject variability, we asked all participants to perform one trial on the same set of randomly chosen 36 triplets. On average, 93.88% of all responses were consistent with majority



Figure 4: In a single trial participants were presented with three different samples. Their task was to compare softness difference between the leftmost and the rightmost pair. Additionally, we placed a force sensor beneath the middle block in order to collect force data throughout the entire experiment.

votes. In the last step, we checked whether subjects could provide consistent ordering of materials, i.e., we sought to avoid orderings such as $D_{ij} < D_{jk} < D_{ik} < D_{ij}$, where D_{ab} is the perceived difference between samples a and b . We randomly chose a set of 12 triples. Subjects were asked to evaluate each of the 3 distance comparisons. We found no cycles in this data.

4.4 Non-metric MDS

In order to find a Euclidean embedding of our metamaterials, we employed non-metric multi-dimensional scaling (NMDS). We use the version proposed by Willis et al. [2009] for building a perceptual space for gloss. Here, we briefly describe how the embedding for our samples was obtained. For more details please refer to the aforementioned work.

Throughout the derivation we use the following notation. Lower case letters $i, j, k \dots$ are used to indicate indices of our samples. Bold lower case letters \mathbf{x} indicate vectors, and upper case letters $P, Q, R \dots$ are used for matrices. Columns of the matrix X denote the embedded coordinates of the samples, and matrix K denotes the Gramian $K = X^\top X$, which is positive semi-definite ($K \succeq 0$).

Unlike metric MDS, where the input data consist of distances between samples, our data contains triplets (i, j, k) , which indicate that the distance between samples i and j was smaller than between j and k . This is denoted as $D_{ij} < D_{jk}$. The goal of NMDS is to find a Euclidean embedding that satisfies as many of the constraints as possible.

One can reformulate the MDS problem using Gramian matrix K as follows. We can write:

$$D_{ij}^2 = \|\mathbf{x}_i - \mathbf{x}_j\|_2^2 = K_{ii} - 2K_{ij} + K_{jj}$$

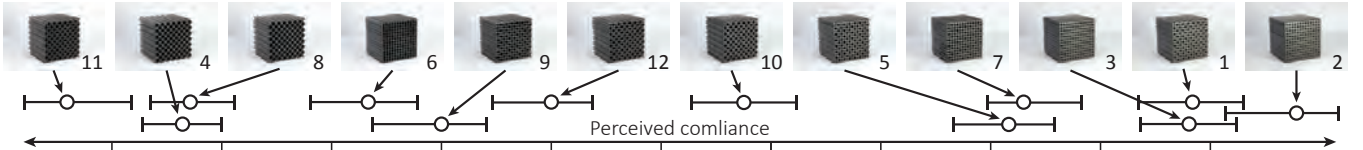


Figure 5: Perceptual space for our 12 metamaterials found using non-metric multi-dimensional scaling. The error bars visualize the confidence obtained using the bootstrapping test. The intervals marked on the axis correspond to 1 JND.

As the distances are always non-negative, we can replace the constraints $D_{ij} < D_{jk}$ with $D_{ij}^2 < D_{jk}^2$. For such constraints our problem of finding the embedding is equivalent to finding a K matrix that satisfies all these constraints. The constraint that K is a Gramian matrix is sufficient and necessary for the matrix to be an inner product for some set of coordinates x. Therefore, the solution of such a problem will always lead to a valid embedding $X = U\Sigma^{1/2}$ for a given eigen decomposition $K = U\Sigma U^\top$ [Wills et al. 2009].

In the raw form the above formulation is insufficient. First of all, the constraints do not uniquely define matrix K, as the constraints are invariant to scaling and translation. In particular, the optimization can collapse the entire space to one point. Another problem is that we want to minimize the dimensionality of the embedding; therefore, we must modify the cost function. We insert an additional term which minimizes the rank of X. This is equivalent to minimizing the rank of K. However, the rank of a matrix is a non-convex term, which complicates the optimization. Lastly, the above formulation seeks a matrix K that satisfies all the constraints. This, apart from the case where all participants are consistent with each other, is impossible.

Wills et al. [2009] accounted for all these problems and proposed the following optimization problem:

$$\begin{aligned} \arg \min_{K, \xi} & \sum_{(i,j,k)} \xi_{ijk} + \lambda \text{tr}(K) \\ \forall (i, j, k) & D_{ij}^2 + 1 \leq D_{jk}^2 + \xi_{ijk} \\ \xi_{ijk} & \geq 0, \quad \sum_{ij} K_{ij} = 0, \quad K \succeq 0. \end{aligned}$$

Instead of reducing the rank of the matrix K, the optimization reduces the trace, as it can be used as an approximation of rank. In order to deal with possible constraint violation, they introduce slack variables ξ_{ijk} . Furthermore, to prevent collapsing the embedding to one point and to remove translation ambiguity, the distance between points is enforced to be at least one and the center of the embedding must be at the origin (second constraint in the third line). In order to solve the above optimization problem we use the SeDuMi 1.05 Optimization Toolbox [Sturm 1999].

4.5 Analysis

The optimization defined in the previous section can find different embeddings depending on parameter λ . To find a space that explains both the observed and the unobserved data well, we perform a cross-validation [Hastie et al. 2009]. At each step we divide the constraints collected in the experiments into two sets: training and testing. Next, we use the training set to optimize for the embedding. In order to find out how well the trained model explains the training data, we compute a training error by counting how many pairwise comparisons from the training set are violated. Similarly, we compute the testing error by counting violations in the testing set. The goal of cross-validation is to find the parameter λ which gives the smallest testing error. We run 10-fold cross-validation. The data set was divided into 10 sets and in each trial, one of them was

treated as a testing set. The errors were averaged across all trials. Figure 6 (left) presents the outcome of this validation as a function of λ . The best trade-off was obtained for $\lambda = 5$ (training error equal to 8.96% and testing error 9.78%). To analyze the dimensionality of this embedding we computed a spread, which describes the variance along each embedding dimension (Figure 6, right). As seen on the plot, almost all variance is contained in the first coordinate. This suggests that the space can be approximated well using only one dimension. The space for the 12 materials from our experiment is shown in Figure 5. We also plot their confidence intervals and scale in just-noticeable units, both described below.

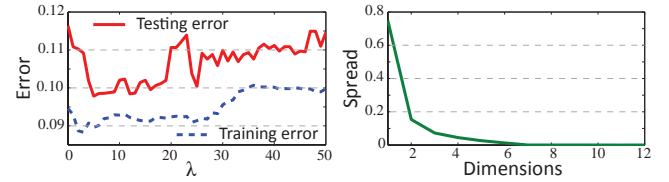


Figure 6: Left: Testing and training error for non-linear MDS as a function of λ parameter. Right: Variance across each embedding dimension (spread) for $\lambda = 5$.

Confidence of the Prediction The data used to compute our perceptual space is influenced by the inherent uncertainty of our psychophysical experiment. The question that arises is how confident we are in said perceptual space. To measure this, we applied a bootstrapping technique [Davison and Hinkley 1997] which allows us to compute confidence intervals for coordinates of our stimuli in the perceptual space. To this end, we computed our perceptual space 1000 times, each time performing resampling of our data with replacement, i.e., the number of measurements that were used in the NMDS was always the same but each time the measurements were chosen randomly with repetitions from our original data. Using this technique, for each stimulus we obtained an estimate of the distribution function of the sample position in the perceptual space. We then compute confidence intervals as the 5th and 95th percentile of this distribution.

JND Estimation The perceptual space allows us to compare differences between samples. However, the units in which they are expressed are undefined. For better understanding of the differences, we scale our prediction in JND (just-noticeable difference) units. A difference of one JND unit is detectable with a probability around 75%. Normally, to obtain the value of 1 JND a threshold estimation experiment needs to be conducted. Such experiments require a continuous change of the stimulus during the experiment. This is unsuitable in our scenario, where modifying stimuli requires reprinting them. Therefore, we decided to use the samples that we already had. We chose four pairs which lie close together in our perceptual space and performed a simple discrimination experiment in which 16 participants were asked to decide which sample in each pair was softer. The results of this experiment (Table 1) suggest that 1 JND unit in our initial perceptual space can be assumed to be around 0.15. Interestingly, as can be observed in Figure 5, 1 JND corresponds

approximately to the size of the confidence intervals, which suggests that the confidence is on the level of human error.

| # SAMPLE 1 | # SAMPLE 2 | Answers | Diff. MDS |
|------------|------------|---------|-----------|
| 7 | 5 | 53 % | 0.0117 |
| 9 | 12 | 76 % | 0.1561 |
| 2 | 3 | 86 % | 0.1738 |
| 8 | 11 | 95 % | 0.2533 |

Table 1: Results of our JND estimation experiment. The first two columns provide block numbers (Figure 2) that were compared by the participants. The third column provides a percentage of people that answered that SAMPLE 1 was softer than SAMPLE 2. The fourth column provides the corresponding difference in our initial perceptual space.

5 Computational Model for Stiffness

The perceptual space derived in the previous section holds for the set of the 12 samples that were used in our experiment. It is unclear how new materials can be embedded in this space. To address this problem, we seek an analytical model that can be evaluated for an arbitrary material. To this end, we tested a number of computational models and compared them with our space. The models we chose are inspired by Pressman et al. [2011], who proposed several models for discrimination tasks of delayed stiffness. Although this is different from compliance of nonlinear materials, the delayed feedback considered in their work also results in a nonlinear relationship between displacement and exerted force. Their models rely directly on data recorded using a haptic device, i.e., force and penetration applied by a user to a virtual material sample. This is crucial because compliance perception depends on the way people interact with objects [Friedman et al. 2008]. To account for the user interaction, we propose to characterize the interaction with materials using peak-force distribution functions. In the following part of this section, we first describe how such information can be acquired. Then, we describe and analyze models that can be used as an explanation of perception of compliant materials.

5.1 Force Distribution

We characterize human interaction with a material using probability distributions of peak-force magnitudes. More precisely, we seek a function $P(f) : \mathbb{R} \rightarrow \mathbb{R}$ which defines the probability that during probing the sample a user will perform a penetration with maximum force equal to f . To this end, we first collected force data as a function of time for each block (Figure 7, left). We did this by placing a force sensor under the reference sample in our experiment (Figure 4). To seek a unified model which predicts perceived compliance for an average observer, we combined force data from all subjects. To approximate function P_i for each material block i , we computed a histogram of peak-force values (Figure 7, red circles) $H_i = (f_{ij}, n_{ij})$, where n_{ij} corresponds to the number of samples in the j -th bin of the histogram centered around force f_{ij} . In this work, we used 16 bins to compute the histograms ($j \in 1, 2, 3 \dots 16$). After normalizing the histograms by the total number of samples, they can be used as an approximation of P_i : $P_i(f_{ij}) = n_{ij} / \sum_{j=1}^{16} n_{ij}$. An example of normalized histograms for two blocks is presented in Figure 7 (right). To see histograms for all blocks, please, refer to the supplemental material.

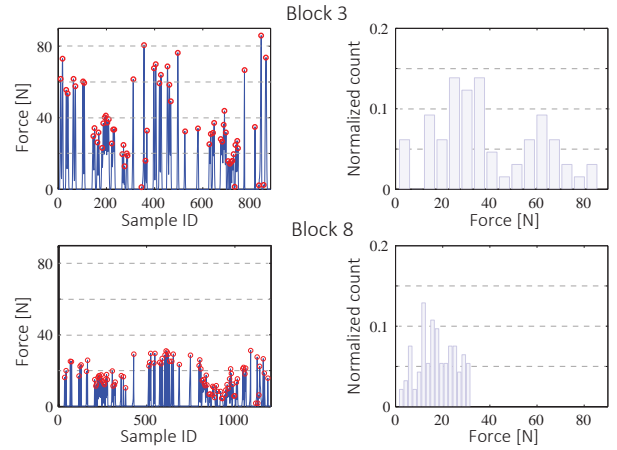


Figure 7: The plots visualize the data collected in our force experiment for blocks 3 and 8. Plots on the left visualize the raw data captured from using our setup: the x-axis corresponds to samples (time), and the y-axis corresponds to the force applied by subjects. The red circles show the peak forces which are used to compute peak-force histograms on the right. As the deformation properties of blocks 3 and 8 differ significantly, the forces applied by users are also different.

5.2 Models

Here, we describe several models that we consider candidates for approximating the perceptual space of compliance found using MDS. We rely on models presented by Pressman et al. [2007] for delayed stiffness, but augment them with the force data. Additionally, we propose modifications which improve the performance of the models in the context of materials considered in this paper.

Global Stiffness (GS) This hypothesis states that people judge the compliance of a material by estimating the local slope of the force-displacement curve, which corresponds to local physical stiffness. In this case, perceived compliance k_i for material i can be estimated using linear regression on the force-displacement data c_i . The assumption is that the slope of the fitted line corresponds to the perceived compliance magnitude. Before performing the regression, the data is truncated to the maximum force applied in the force estimation experiment, i.e., the regression is performed on corresponding c_i but only for forces smaller than maximum force applied f_{max} , where $P_i(f) < 0$ for each $f < f_{max}$.

$$k_i = \arg \min_k \int_0^{c_i^{-1}(f_{max})} (kx + b - c_i(x))^2 dx \quad k, b \in \mathbb{R}.$$

Here, $c_i^{-1}(f)$ corresponds to the penetration distance for a given force f . Additionally, we introduce an alternative version of this model where the linear function fitted to the data passes through the origin GSF (Global Stiffness Fixed), i.e., $b = 0$. Good performance of this model could suggest that people, while estimating stiffness of a given material, account for the fact that zero-force should result in no displacement. Therefore, the estimated slopes should correspond to a linear function intersecting the origin.

Local Stiffness (LS) This model also estimates the compliance as a slope of the linear fit to the force-displacement curve, but to further include the force data, we use weighted least-square regression, where weights correspond to values of peak-force probability, i.e.,

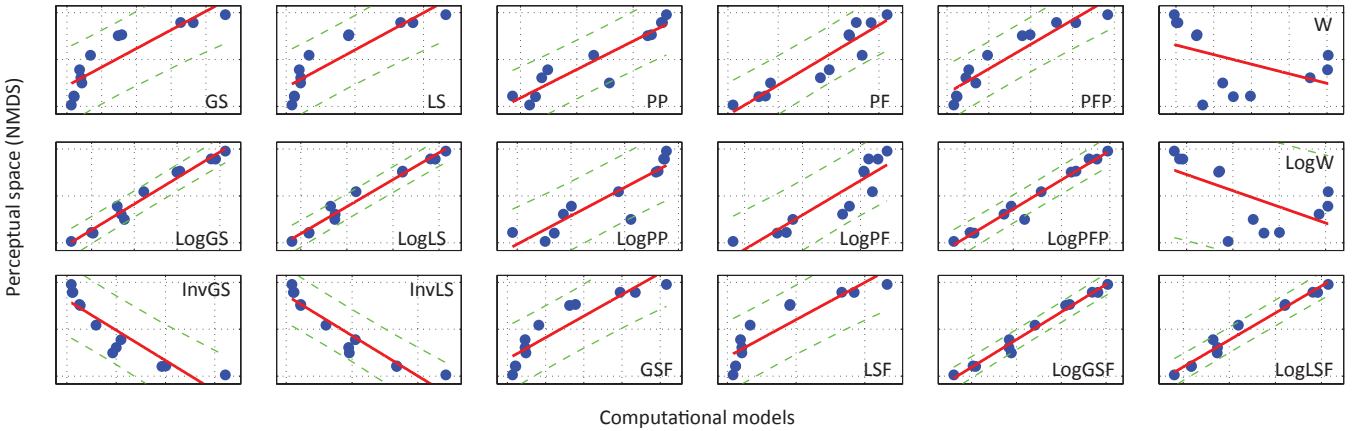


Figure 8: The plots show how different computational models correlate with the perceptual space obtained using non-metric multi-dimensional scaling. Each chart's X and Y axis correspond to computational model and perceptual space, respectively. Blue points correspond to our stimuli. The red lines are the results of the linear regression and the green dashed lines indicate prediction intervals with a confidence level of 0.95. A good correlation between computational models and experimental data was found for several models.

| | GS | LS | PP | PF | PFP | W | LogGS | LogLS | LogPP | LogPF | LogPFP | LogW | InvGS | InvLS | GSF | LSF | LogGSF | LogLSF | L2 |
|----------|-------|-------|-------|-------|-------|-------|--------------|--------------|-------|-------|--------------|-------|-------|-------|-------|-------|--------------|--------------|-------|
| R^2 | 0.786 | 0.813 | 0.866 | 0.871 | 0.883 | 0.206 | 0.973 | 0.975 | 0.820 | 0.812 | 0.969 | 0.368 | 0.813 | 0.892 | 0.841 | 0.813 | 0.984 | 0.975 | – |
| vs. data | 83.1% | 85.3% | 83.8% | 82.8% | 87.7% | 63.5% | 90.3% | 91.2% | 83.5% | 82.7% | 91.1% | 67.1% | 86.1% | 90.3% | 86.2% | 85.3% | 92.2% | 92.3% | 91.1% |
| vs. MDS | 83.8% | 86.9% | 84.4% | 82.5% | 88.0% | 65.5% | 90.6% | 92.9% | 84.1% | 82.3% | 92.4% | 69.0% | 85.7% | 91.2% | 86.5% | 86.9% | 92.5% | 92.9% | 92.1% |

Table 2: Statistics from experiments evaluating each computational model. High values marked in bold indicate good candidates for computational models. Each of them does a good job of predicting not only the distances evaluated using the perceptual space found using MDS (above 90%), but also the data collected in our main experiment.

the error of the fit is weighted by $P_i(f)$ for each force f :

$$k_i = \arg \min_k \int_0^{c_i^{-1}(f_{max})} P_i(c_i(x)) \cdot (kx + b - c_i(x))^2 dx \quad k, b \in \mathbb{R}.$$

This formulation requires a continuous function P . For the purpose of this work, it is approximated using a discrete summation over the peak-force histograms. In the case of 16 histogram bins, the compliance can be computed as:

$$k_i = \arg \min_k \sum_{j=1}^{16} n_{ij} \cdot (kx + b - f_{ij})^2 dx \quad k, b \in \mathbb{R}.$$

Analogously to GSF model, we also define *Local Stiffness Fixed* (LSF) by enforcing $b = 0$.

Maximum Displacement (MD) This model, as proposed in [Pressman et al. 2007], estimates compliance using maximum displacement during one penetration. We propose to compute an expected value of maximum displacement. Hence, we define it as follows:

$$k_i = \int_0^{\infty} P_i(f) \cdot c_i^{-1}(f) df.$$

Maximum Force (MF) Analogous to the previous model, this estimated the compliance as an expected value of force exerted on a given material:

$$k_i = \int_0^{\infty} P_i(f) \cdot f df.$$

Peak Force/Penetration ratio (PFP) As originally proposed, this model estimates the compliance as a ratio between peak-force during a single interaction and the corresponding displacement. Analogously to the previous model, we define this model as an expected

value of this quantity:

$$k_i = \int_0^{\infty} P_i(f) \cdot \frac{f}{c_i^{-1}(f)} df.$$

Work (W) Inspired by the experiment of Jones and Hunter [1990], which showed that work is an important cue when discriminating stiffness, we added work as another hypothetical model for compliance. In this case, we define it as expected work that is done during a single penetration motion:

$$k_i = \int_0^{\infty} P_i(f) \cdot \int_0^{c_i^{-1}(f)} c_i(x) dx df.$$

Additional Variations As suggested by Leib et al. [2010] the compliance of nonlinear materials may relate to an inverse slope of the linear function fitted to the force-displacement curve. To investigate this hypothesis, we considered models INVGS and INVLS which are inverses of the previously defined models GS and LS.

It has been previously observed that for linear materials, the mechanical stiffness obeys the Weber law [Tan et al. 1992]. This suggests that the same may hold for the above models. In order to test this hypothesis, we added models which measure compliance as a logarithm of previously described quantities: LOGGS, LOGLS, etc.

5.3 Analysis

In order to validate which of the above computational models best explains compliance perception, we compare the prediction of each model with the perceptual space found in Section 4. To this end, for each computational model, we compute the coordinates of all 12 blocks and check how these coordinates correlate with those from the perceptual space. Our assumption is that a computational model

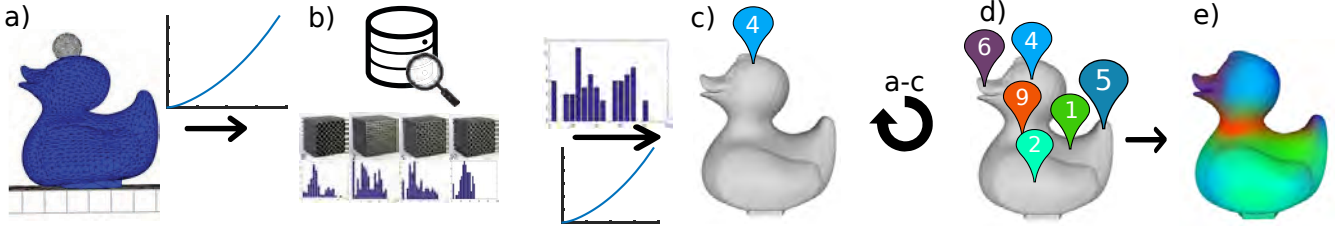


Figure 9: To compute compliance properties of an object we start with simulating the interaction performed by an observer for a given location on the surface (a). This allows us to extract force-displacement information. Next, the force histogram is obtained using our database of blocks with ground-truth force information (b). To this end, we interpolate histograms corresponding to the two closest curves in the database. Given the force-displacement curve together with the corresponding force histogram, compliance properties are computed according to our model (c). The procedure is repeated for a set of locations on the surface (d). To obtain a dense, spatially-varying compliance map, we interpolate the compliance values on the object’s surface (e).

is good only if its outcome has good linear correlation with the perceptual space. To measure the correlation we use linear regression. Figure 8 visualizes the results of this experiment for all computational models. The goodness of the fit for each model was measured using R-squared. The values are presented in Table 2. As we are not only interested in a good prediction of perceived compliance, but also perceived distances, we also check how computational models predict differences in pairwise distances between materials. To this end, we computed what percentage of experimental data (Section 4) is explained by each model. We performed the same test assuming that all triplets from the main experiment were evaluated using our perceptual model. For validating distances we also include the L2 norm on displacements evaluated on force-displacement curves proposed by Bickel et al. [2010]. The results of these experiments are presented in Table 2.

The results indicate that there are five models that provide a good match with both the data obtained in the experiment and the perceptual spaced found using MDS. The fact that all these models are logarithmic supports the Weber-law hypothesis. Surprisingly, a simple L2 norm can also provide a good prediction of differences in pairwise distances (see last column of Table 3). To investigate this further we checked how well the distances in the perceptual space are explained by our models and the L2 norm. To this end, we considered all pairwise distances between our 12 stimuli and computed their magnitude using the perceptual space, our models, and the L2 norm. We then computed a correlation between the observed distances in the perceptual space and the predicted ones. Table 3 shows the correlation for the five best performing models evaluated in this paper as well as the L2 norm. The correlation for the L2 norm turned out to be worse than for our perceptually-motivated models. In Figure 10, we also show plots of predicted versus observed distances for LogLSF and L2.

| LogGS | LogLS | LogPFP | LogGSF | LogLSF | L2 |
|-------|-------|--------|--------|--------|------|
| 0.96 | 0.96 | 0.96 | 0.97 | 0.98 | 0.89 |

Table 3: Correlation between distances in the perceptual space and the prediction provided by the computational models and the L2 norm.

To summarize, our analysis suggests that five of the models tested in our experiments (LogGS, LogLS, LogPFP, LogGSF, LogLSF) perform well in predicting the perceptual space found in Section 4. Three of these models (LogGS, LogLS, LogPFP) were also found to perform well for perception of delayed stiffness of linear materials [Pressman et al. 2007]. However, in our case where we seek a perceptual space, we had to consider the logarithm of the corresponding quantities; otherwise the prediction was poorer. Furthermore, to ac-

count for differences in user interaction, we augmented these models with additional force information. The best performance was provided by LogLSF, which was not considered by Pressman et al. Surprisingly, the non-perceptual L2 norm performed well in predicting the relation between pairwise distances; however, it performed worse in predicting the magnitude of the differences.

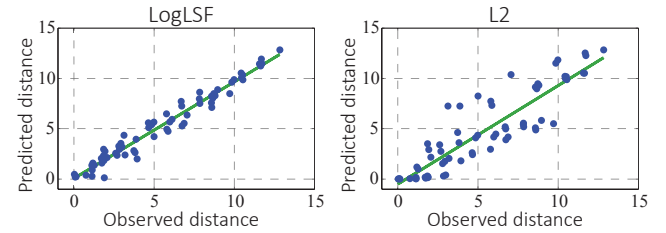


Figure 10: The two plots visualize the distance prediction between our stimuli as predicted by the LogLS model and the L2 norm with respect to the observed distances in the perceptual space. LogLS outperforms the L2 norm by providing a much closer match to the observed distances.

6 Complex Geometries

In the previous section, we considered different models for modeling compliance perception. Their performance was analyzed based on the data collected for simple shapes, i.e., blocks made of different metamaterials. In this section, we demonstrate how such models can be applied to complex geometries. In the rest of the paper, we will use the LogLSF model as it performed best in our analysis in Section 5.

6.1 Computational Model for Complex Geometries

Compliance perception depends on the force-displacement relationship at the point of contact with an object. As such, it is influenced not just by the material an object is made of, but by its shape as well. Figure 9 outlines our method for extending our model to complex geometries using numerical simulation of elastic objects.

Compliance Computation To predict the perceived compliance at a given contact location \mathbf{x} on the object’s surface, we first have to determine the force-displacement curve. In the case of real objects, such information can be obtained using a uniaxial test with force applied at the point \mathbf{x} . For fabrication applications we must estimate this information before the object is produced; to do this, we rely on numerical simulations. We simulate poking an object with a finger-like contact geometry in the direction of the contact surface

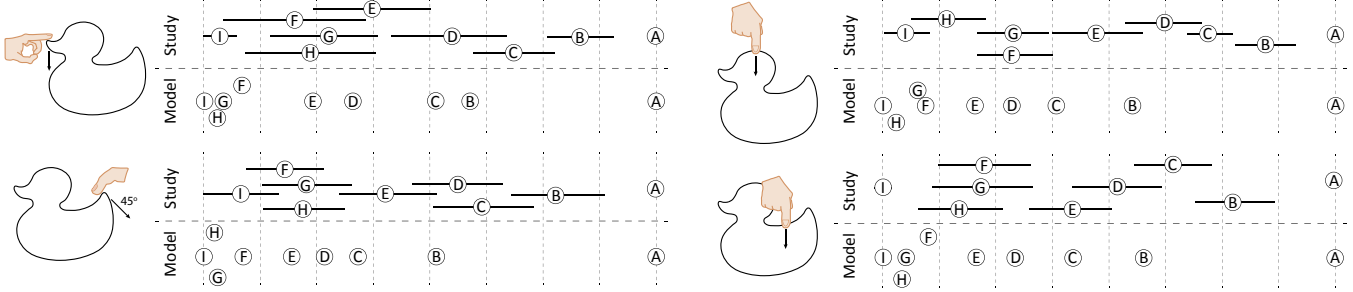


Figure 11: The results of the evaluation of our compliance model. The plots visualize the compliance as judged by the participants (top row), as well as our prediction (bottom row). Additionally, the schematic figures visualize the mode of interaction. Letters A-I correspond to different silicon mixtures ordered by Shore hardness. For more details about materials used please refer to the supplementary material.

normal, (Figure 9a). Recording both the force and displacement of the contact patch produces a holistic force-displacement curve for the entire object. In addition to the force-displacement information, our model requires a force histogram that describes the interaction of a subject with the object. Here, we rely on the prediction based on the data collected in our experiments with blocks (Section 4). We assume that subjects interact in a similar way with objects that have similar force-displacement characteristics. Consequently, to predict the histogram for a new force-displacement curve, we first find two blocks that have the most similar force-displacement curves in our database (Figure 9b). The distance between curves is measured as the area between them, though any metric could be used. Then, we interpolate the two corresponding force histograms using the distances as weights. For the interpolation we use the method proposed by Bonneel et al. [2011]. Next, given the force-displacement curve and the force histogram, we can directly apply our model from Section 5 to obtain the prediction of perceived compliance at location x (Figure 9c). In order to compute a dense compliance map for the entire object, we sample its surface using Poisson disk sampling [Cook 1986] and compute local compliance for each location separately (Figure 9d). Later, we interpolate the results using inverse distance weighting. The distance between vertices is measured with an approximation of geodesic distance using the Floyd-Warshall algorithm. A result of such computation is presented in Figure 9e.

Compliance Metric Dense compliance maps allow us to formulate a metric that predicts compliance differences between two objects with the same geometry but made of different materials. To this end, we first compute a dense compliance map for both objects which are then subtracted. As the compliance prediction provides information in perceptually uniform units, the direct differences are perceptually meaningful and their magnitude can be interpreted as perceived differences. An example of such a map is presented in Figure 12.

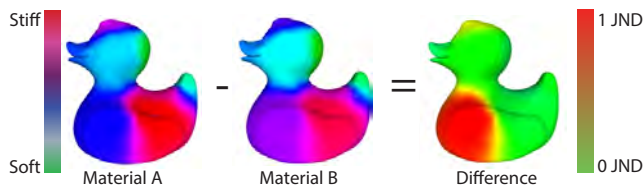


Figure 12: To compute difference between two versions of the same object made of two different materials, we first compute a compliance map for each of them. Then, we subtract the values corresponding to the same locations. Here, Material A and Material B correspond to silicones with Young's modulus values of 0.0964 MPa and 0.0973 MPa, respectively.

6.2 Evaluation

To evaluate our strategy for computing compliance properties of complex geometries, we conducted a user experiment, in which participants investigated objects with different mechanical properties and were asked to judge the differences between them. The outcome of the experiment was compared to predictions provided by our model and the L2 norm.

Stimuli For the purpose of this experiment, we used a duck-toy shape for which we printed a mold and cast the shape with 9 different mixtures of silicones (Figure 1). This way we obtained shapes with different mechanical properties. The size of each duck was approximately $7 \times 6.5 \times 4.5$ cm. Additionally, for each silicone we cast a small cube that was used to measure the nominal stress-strain curves for each material, which were later used for physically-based simulation of the shapes. For more details about the physical simulation and materials used please refer to the supplementary material.

Experiment Ten participants took part in this experiment. Each of them was presented with all the stimuli at once and asked to order the objects according to compliance. Participants were allowed to palpate the object at a prescribed location in a direction perpendicular to the surface. To acquire information about perceived differences between the objects, we asked participants to space the objects according to the differences between them. For this purpose they were asked to arrange the objects along a 2 meter scale. We chose four different locations which subjects were asked to evaluate: head, tip of the beak, body, and tail. Each participant performed the experiment in four separate sessions. This allowed us to reduce the bias introduced by previous examinations of different locations. To make the scenario realistic, we did not prevent visual feedback.

Results Each subject provided four orderings. For each of them the positions were recorded, scaled to 0–1 range, and averaged across the participants. As a result, we obtained four orderings together with relative positions. We also predicted the perceived compliance using our model and compared them to the subjective evaluation. The results of this analysis are presented in Figure 11. To evaluate how good our prediction is, we computed Spearman's rank correlation and Pearson's correlation coefficients between the positions from the subjective experiment and the prediction. They are equal to 0.9617 and 0.9269, respectively. For computational fabrication techniques, such as [Bickel et al. 2010; Chen et al. 2013] more relevant information is the differences between objects. To evaluate our model in this context, we compare its prediction to the L2 norm which is often used in practice. To this end, we computed all pairwise distances between the objects according to our model,

the L2 norm, and the positions provided by the participants. Table 4 presents coefficients for Pearson’s correlations between the user data and our prediction as well as the user data and the L2 norm for each location separately.

| | Beak | Head | Tail | Body |
|--------------------|--------|--------|--------|--------|
| L2 vs. Exp. data | 0.6541 | 0.6378 | 0.7657 | 0.6092 |
| Ours vs. Exp. data | 0.9090 | 0.8952 | 0.8959 | 0.8490 |

Table 4: Correlation between distances predicted by our method and the L2 norm.

Discussion The evaluation shows that our prediction correlates well with the positions and distances obtained from our user experiment. This suggests that the computational model that we propose in this paper can be used for judging the perceived compliance and distances between objects with different mechanical properties. Additionally, we show that our model outperforms a simple L2 norm operating directly on force-displacement data. When compared to the results obtained for simple shapes (Section 5, Table 3), the correlation coefficients for complex geometries (Table 4) are lower. We believe that this reduced performance can be attributed to: (a) accuracy of the interaction performed by participants (i.e., contact position and direction of interaction), and (b) the contact area of the finger and the object, which depends on the neighborhood of the point of interaction.

Using our data, we can also evaluate whether or not the perceived compliance depends on the geometry or solely on the material properties of an object. To test the hypothesis that the geometry influences perception, we computed two-way analysis of variance (ANOVA) on our data from the experiment. The two variables considered in the test were the location of the interaction and the silicone used for casting the shapes. The ANOVA revealed a significant effect for both variables with $p < 0.05$. This shows that people are not able to factor out the geometry while judging the mechanical properties of the object, and that our approach that takes into account this factor is justified.

7 Application to 3D Printing

In this section we propose three possible usage scenarios for our model. First, we show that it can help in the process of choosing the right material for fabricating objects with prescribed compliance properties. The second use case demonstrates that our compliance prediction can speed up prototyping processes by providing suggestions to designers. Finally, we discuss how our model can affect current state-of-the-art fabrication algorithms.

7.1 Accuracy

Reproducing desired deformation properties is an important problem. Recent work tackles this problem by fabricating metamaterials made of micro-structures [Bickel et al. 2010; Schumacher et al. 2015; Panetta et al. 2015]. However, due to the limitations imposed by designers or 3D printers, complex internal structures are not always desirable or fabricable. In practice, the designer might be able to use only a limited number of materials to reproduce a target object. As shown in previous sections, our model has a higher correlation with user data than the L2 norm, which suggests that one could use it to improve the accuracy of optimization for material assignment.

Experiment To examine this claim, we conducted the following experiment. We fabricated a seahorse model using five different materials: TangoBlack+ (Objet500 Connex), TPU 92A-1 (Laser



Figure 13: From left to right: a rendering of the original seahorse model. Seahorse models used for the study: Dragon Skin 30, Ecoflex 00-30, TangoBlack+, Flexible resin, TPU 92A-1.

printer), Flexible resin (Ember printer), Smooth-On Dragon Skin 30 silicone rubber (casting), and Smooth-On Ecoflex 00-30 silicone rubber (casting) shown in Figure 13. The experiment consisted of generating all triplets of materials. From each triplet the object with medium stiffness was removed and the task was to decide which of the two remaining materials should be used to replicate the removed object. We assumed that during interaction each seahorse is held by its body and participants examine the tip of its mouth. In total we had 10 trials. In 4 of these trials the L2 norm and our model did not predict the same material. We conducted a user study with 16 participants. All of them were presented with each triplet and asked to choose the best replica.

Results Detailed results of this study are presented in Table 5. The L2 norm correctly predicted 85 out of a total of 160 selections (53%), which is on the level of a random guess. In contrast, our model was able to predict 125 answers (78%). The prediction was always consistent with the majority vote. This suggests that during the design process our model can provide meaningful suggestions to artists regarding the material choice. The L2 norm failed to predict the correct answers in some cases. All of them involved situations when the harder material was the correct answer.

| Material | People | Reference material | Less similar sample | |
|----------------|--------|--------------------|---------------------|--------|
| | | Material | Material | People |
| Dragon Skin 30 | 100% | TangoBlack+ | Ecoflex 00-30 | 0% |
| Ecoflex 00-30 | 69% | TangoBlack+ | TPU 92A-1 | 31% |
| Ecoflex 00-30 | 81% | Dragon Skin 30 | TPU 92A-1 | 19% |
| TPU 92A-1 | 69% | Flexible resin | Dragon Skin 30 | 31% |
| Ecoflex 00-30 | 56% | Dragon Skin 30 | Flexible resin | 44% |
| TPU 92A-1 | 94% | Flexible resin | Ecoflex 00-30 | 6% |
| TangoBlack+ | 88% | Dragon Skin 30 | Flexible resin | 12% |
| Ecoflex 00-30 | 69% | TangoBlack+ | Flexible resin | 31% |
| TangoBlack+ | 94% | Dragon Skin 30 | TPU 92A-1 | 6% |
| TPU 92A-1 | 63% | Flexible resin | TangoBlack+ | 37% |

Table 5: Results of the perceptual study. From each trial the triplet is shown as well as the corresponding participants’ picks. Our predictions always correspond to the participants’ choices. Cases when the L2 norm did not agree with our prediction are highlighted in red.

7.2 Material Selection for Prototyping

Recent advances in 3D printing enable designers to rapidly fabricate and test prototype versions of their designs. However, printing a single prototype can still take hours and consume a considerable amount of material. Therefore, it is desirable to optimize for the cost and the printing time by minimizing the number of printed models. In the context of compliance, the material properties are not very meaningful in the perceptual sense, and the variation of material parameters does not always result in the expected changes in the object behavior due to the geometry of printed models. Our model can help in this process by providing suggestions about the material parameters to designers.



Figure 14: Left: a rendering of the original octopus model. Right: all printed octopuses ordered by stiffness.

Experiment We consider a situation of fabricating an object with unspecified compliance properties. A designer does not know the exact material parameters, and therefore, they wish to print a few versions of the object from which they can choose. To aid the process, it is desired to print objects that will cover the range of the possible outcomes in a uniform way. For the purpose of demonstration we considered an octopus shaped toy (Figure 14, left) that is to be printed on the Objet500 Connex printer. Using digital materials composed from TangoBlack+ and VeroClear one can fabricate 8 different models. To simulate the design process, we conducted an experiment in which 20 participants were asked to put themselves in the role of the designer. They had already tried models with the two base materials and now would like to print some in-between samples. Due to time and cost limitations they can, however, print only a limited subset of the samples. Their task is to pick these samples such that they maximize the difference in compliance between each other. In the first trial users were asked to pick 2 out of 6 possible samples and in the second trial they were allowed to pick 3. To check whether our model can help them in this task, we predicted the user selection by taking sets of samples that maximize the minimal distance measured with our model. For the comparison, we also used the L2 norm.

Results The outcome is presented in Table 6. For the trial of picking two representative samples, the L2 norm predicted the pair 4,2 while our model predicted the pair 6,4. For the trial of picking three samples, our model predicted the triplet 8,6,4 while the L2 norm predicted the triplet 6,4,2. The prediction of our model was always the set with the highest occurrence count; meanwhile, the L2 norm matched people's choice only partially. This demonstrates that our model can be used for designing pallets of materials/objects that exhibit sufficient variation in perceived compliance. The main difference between our model and the L2 norm is that in both trials the L2 norm is biased towards stiffer samples. This is similar to the previous experiment and may suggest that the L2 norm overestimates human sensitivity to hard materials.

| Picking 2 samples | | | | | |
|------------------------|--|--------------------------------------|--|--|---|
| People's choice | 6,4 | 7,4 | 7,6 | 8,6 | ... |
| Probability of choice | 30% | 20% | 20% | 15% | ... |
| Picking 3 samples | | | | | |
| People's choice | 8,6,4 | 7,6,4 | 9,6,4 | 8,7,4 | ... |
| Probability of choice | 35% | 20% | 10% | 10% | ... |
| Our prediction | 6,4 | 7,4 | 8,6 | 9,6 | 10,7,4 |
| The L2 norm prediction | 4,2 | 6,4 | 6,4,2 | 7,6,4 | 8,6,4 |

Table 6: Results of the perceptual study. For both trials of picking two and three samples we present the people's choice and its corresponding probability. Sets predicted by our model and the L2 norm are underlined in green and red, respectively.

7.3 Improving Fabrication Algorithms

Optimizing material/metamaterial assignment in order to obtain desired mechanical properties for a given object is a computationally expensive operation. We have already demonstrated that our model provides a more accurate prediction of differences between objects with respect to the L2 norm. This suggests that we can replace the L2 model in fabrication methods, such as Spec2Fab [Chen et al. 2013], and obtain a closer match (in the perceptual sense) with the desired mechanical properties. However, our model can also shorten the time that such an optimization requires. Given desired properties of an object, we can run and terminate such optimizations when the error drops below one just-noticeable difference.

Experiment To test this hypothesis we ran two Spec2Fab [Chen et al. 2013] optimizations that minimized the L2 norm. One of them was performed until convergence, while the other was stopped when the error measured using our model reached one JND. The resulting curves can be seen in Figure 15. Sixty-four simulation steps were required for the optimization to converge, while only nine simulations were needed for the solution obtained using the perceptual cutoff. Interestingly, when we compute the perceptual difference between target and optimized curves, the converged curve has an error above one JND. Meanwhile, the curve for the terminated optimization has an error under half JND. This indicates that the curve obtained with the perceptual cutoff is a much better reproduction.

Discussion This behavior can be explained by two facts. First, our model takes into account user interaction. Second, it investigates the slope of the force-displacement relation instead of the direct difference between curves. In Figure 15 (left), we can see the plot of force-displacement data for the target object as well as the optimized ones. On the right, we present plots of the corresponding slope values (derivatives). One can clearly see that in the region of main interaction between 18 and 35 N (high values of force histogram), the curve obtained with the perceptual cutoff provides almost a perfect match in terms of the slope. This gives us an important insight about how our model could be used to design new fabrication techniques that optimize the perceived differences directly.

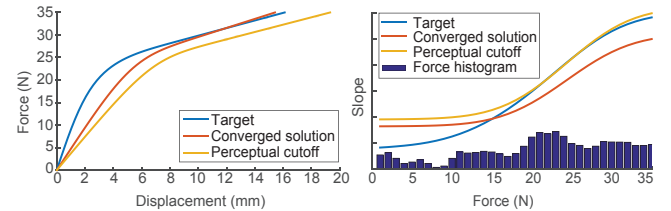


Figure 15: Left: force-displacement curves obtained from Spec2Fab optimization. Right: Slopes of the force-displacement curves along with corresponding histogram of forces.

8 Limitations and Future Work

In our experiments, we demonstrated that the compliance model and metric presented in this paper can be successfully used in many fabrication-oriented applications. However, there are some limitations to our technique.

Our model was constructed using only 12 samples. However, our experiments demonstrated that they cover the compliance range well (Figure 5) and the model achieves good correlation with the measured data. Furthermore, our experiments showed that our model extends beyond the original stimuli database for both softer (e.g.,

Ecoflex 00-30) and harder (e.g., VeroClear) materials.. The limited number of materials was also a design choice. More samples would make our user study infeasible. We believe that it is straightforward and beneficial to extend the force histograms database to improve the performance of our technique for complex geometries.

More limiting than the above, our model only supports a single mode of interaction (poking). We limit ourselves to elastic material models which assume no velocity dependence on resulting forces. Although for many of the materials used in our applications (i.e., silicones, Flexible resin, TPU 92A-1) this is acceptable, for some viscoelastic 3D printable materials, e.g., TangoBlack+, this is not an ideal assumption. Visual feedback was avoided for the purpose of modeling compliance perception in Sections 4 and 5. For practical reasons we did not avoid it during evaluation of the applications for complex geometries. We restricted our study to nonlinearly elastic materials that were produced by 3D printing metamaterials. Although they cannot be considered as natural materials, the benefit of using them for such experiments is the fact that people are unfamiliar with them. Therefore, additional cues such as textures are eliminated. An obvious direction of future work would be to relax one or more of these assumptions. Exploring free-form interactions or more complex material models could be particularly interesting, as they may result in a higher-dimensional perceptual space. Incorporating modeling of visual and texture feedback may further improve the performance of our model in fabrication applications.

The other set of limitations comes from how the perceptual model was applied to complex geometries. In particular, for each point on the surface, we examine only a single poking direction perpendicular to the object's surface. While this is a natural direction for poking, in practice it is nearly impossible to poke objects exactly along the normal of the surface. This can negatively affect the compliance prediction of very complex objects where even a slight deviation from the normal direction results in perceptually different compliance properties. To apply our model in such a case, one could simulate the interaction for multiple poking directions and integrate the individual predictions to get the resulting compliance. How to integrate those predictions is an interesting problem for future work. Such integration of compliance would require prior knowledge of the interaction and the ability to predict which poking directions are more probable than others.

9 Conclusions

We presented a psychophysical experiment for evaluating compliance of different materials. Based on the collected data, we found a perceptual embedding of 12 blocks of metamaterials. Our results suggest that despite the high dimensionality of possible nonlinear materials, the perceptual space can be estimated well using a one-dimensional embedding. This may suggest that people try to relate nonlinear materials to corresponding linear materials. The perceptual space was later used to evaluate different computational models for predicting perceived compliance. Based on the above experiments and modeling, we proposed an interaction-aware compliance model which is capable of estimating perceived differences between compliant 3D objects. We also demonstrated several applications that showcase the capabilities of our model. Both the model and the applications are evaluated in a series of user experiments. The proposed model can be easily integrated in many existing computational fabrication algorithms, such as [Bickel et al. 2010; Chen et al. 2013; Schumacher et al. 2015; Panetta et al. 2015].

References

- AMBROSI, G., BICCHI, A., ROSSI, D. D., AND SCILINGO, E. P. 1999. The role of contact area spread rate in haptic discrimination of softness. In *Robotics and Automation, 1999. Proceedings. 1999 IEEE International Conference on*, vol. 1, 305–310 vol.1.
- BERGMANN TIEST, W. M., AND KAPPERS, A. M. 2006. Analysis of haptic perception of materials by multidimensional scaling and physical measurements of roughness and compressibility. *Acta psychologica* 121, 1, 1–20.
- BICKEL, B., BÄCHER, M., OTADUY, M. A., LEE, H. R., PFISTER, H., GROSS, M., AND MATUSIK, W. 2010. Design and fabrication of materials with desired deformation behavior. *ACM Transactions on Graphics (TOG)* 29, 4, 63.
- BONNEEL, N., VAN DE PANNE, M., PARIS, S., AND HEIDRICH, W. 2011. Displacement interpolation using lagrangian mass transport. *ACM Trans. Graph.* 30, 6, 158:1–158:12.
- CHEN, D., LEVIN, D. I., DIDYK, P., SITTHI-AMORN, P., AND MATUSIK, W. 2013. Spec2fab: a reducer-tuner model for translating specifications to 3D prints. *ACM Transactions on Graphics (TOG)* 32, 4, 135.
- COOK, R. L. 1986. Stochastic sampling in computer graphics. *ACM Trans. Graph.* 5, 1 (Jan.), 51–72.
- COOKE, T., KANNENGIESSER, S., WALLRAVEN, C., AND BÜLTHOFF, H. H. 2006. Object feature validation using visual and haptic similarity ratings. *ACM Transactions on Applied Perception (TAP)* 3, 3, 239–261.
- COOKE, T., WALLRAVEN, C., AND BÜLTHOFF, H. H. 2010. Multidimensional scaling analysis of haptic exploratory procedures. *ACM Transactions on Applied Perception (TAP)* 7, 1, 7.
- DAVISON, A. C., AND HINKLEY, D. V. 1997. *Bootstrap Methods and their Application*. Cambridge University Press.
- FRIEDMAN, R. M., HESTER, K. D., GREEN, B. G., AND LAMOTTE, R. H. 2008. Magnitude estimation of softness. *Experimental brain research* 191, 2, 133–142.
- GENECOV, A. M., STANLEY, A. A., AND OKAMURA, A. M. 2014. Perception of a haptic jamming display: Just noticeable differences in stiffness and geometry. In *Haptics Symposium (HAPTICS), 2014 IEEE*, IEEE, 333–338.
- GKIOULEKAS, I., XIAO, B., ZHAO, S., ADELSON, E. H., ZICKLER, T., AND BALA, K. 2013. Understanding the role of phase function in translucent appearance. *ACM Transactions on Graphics (TOG)* 32, 5, 147.
- HAN, D., AND KEYSER, J. 2015. Effect of appearance on perception of deformation. In *Proceedings of the 14th ACM SIGGRAPH / Eurographics Symposium on Computer Animation*, ACM, New York, NY, USA, SCA '15, 37–44.
- HARPER, R., AND STEVENS, S. 1964. Subjective hardness of compliant materials. *Quarterly Journal of Experimental Psychology* 16, 3, 204–215.
- HASTIE, T., TIBSHIRANI, R., FRIEDMAN, J., HASTIE, T., FRIEDMAN, J., AND TIBSHIRANI, R. 2009. *The elements of statistical learning*, vol. 2. Springer.
- HOLLINS, M., BENNSMAÏA, S., KARLOF, K., AND YOUNG, F. 2000. Individual differences in perceptual space for tactile textures: Evidence from multidimensional scaling. *Perception & Psychophysics* 62, 8, 1534–1544.

- JONES, L. A., AND HUNTER, I. W. 1990. A perceptual analysis of stiffness. *Experimental Brain Research* 79, 1, 150–156.
- KOÇAK, U., PALMERIUS, K. L., FORSELL, C., YNNERMAN, A., AND COOPER, M. 2011. Analysis of the JND of stiffness in three modes of comparison. In *Haptic and Audio Interaction Design*. Springer, 22–31.
- KUSCHEL, M., DI LUCA, M., BUSS, M., AND KLATZKY, R. L. 2010. Combination and integration in the perception of visual-haptic compliance information. *Haptics, IEEE Transactions on* 3, 4, 234–244.
- LEDERMAN, S. J., AND KLATZKY, R. L. 2009. Haptic perception: A tutorial. *Attention, Perception, & Psychophysics* 71, 7, 1439–1459.
- LEIB, R., NISKY, I., AND KARNIEL, A. 2010. Perception of stiffness during interaction with delay-like nonlinear force field. In *Haptics: Generating and Perceiving Tangible Sensations*. Springer, 87–92.
- LEŠKOWSKÝ, P., COOKE, T., ERNST, M. O., AND HARDERS, M. 2006. Using multidimensional scaling to quantify the fidelity of haptic rendering of deformable objects. In *Proceedings of the EuroHaptics 2006 International Conference (EH 2006)*.
- MISRA, S., FUERNSTAHL, P., RAMESH, K., OKAMURA, A. M., AND HARDERS, M. 2009. Quantifying perception of nonlinear elastic tissue models using multidimensional scaling. In *Euro-Haptics conference, 2009 and Symposium on Haptic Interfaces for Virtual Environment and Teleoperator Systems. World Haptics 2009. Third Joint*, IEEE, 570–575.
- MOROVIC, J., AND LUO, M. R. 2001. The fundamentals of gamut mapping: A survey. *Journal of Imaging Science and Technology* 45, 3, 283–290.
- NISKY, I., PRESSMAN, A., PUGH, C. M., MUSSA-IVALDI, F. A., AND KARNIEL, A. 2011. Perception and action in teleoperated needle insertion. *Haptics, IEEE Transactions on* 4, 3, 155–166.
- PANETTA, J., ZHOU, Q., MALOMO, L., PIETRONI, N., CIGNONI, P., AND ZORIN, D., 2015. Elastic textures for additive fabrication, aug. Julian Panetta and Quingnan Zhou are Joint first authors.
- PELLACINI, F., FERWERDA, J. A., AND GREENBERG, D. P. 2000. Toward a psychophysically-based light reflection model for image synthesis. In *Proceedings of the 27th annual conference on Computer graphics and interactive techniques*, ACM Press/Addison-Wesley Publishing Co., 55–64.
- PRESSMAN, A., WELTY, L. J., KARNIEL, A., AND MUSSA-IVALDI, F. A. 2007. Perception of delayed stiffness. *The International Journal of Robotics Research* 26, 11-12, 1191–1203.
- PRESSMAN, A., KARNIEL, A., AND MUSSA-IVALDI, F. A. 2011. How soft is that pillow? The perceptual localization of the hand and the haptic assessment of contact rigidity. *The Journal of Neuroscience* 31, 17, 6595–6604.
- REINHARD, E., HEIDRICH, W., DEBEVEC, P., PATTANAIK, S., WARD, G., AND MYSZKOWSKI, K. 2010. *High dynamic range imaging: acquisition, display, and image-based lighting*. Morgan Kaufmann.
- REN, Z., YEH, H., KLATZKY, R., AND LIN, M. C. 2013. Auditory perception of geometry-invariant material properties. *Visualization and Computer Graphics, IEEE Transactions on* 19, 4, 557–566.
- SCHUMACHER, C., BICKEL, B., RYS, J., MARSCHNER, S., DARAIO, C., AND GROSS, M. 2015. Microstructures to control elasticity in 3D printing. *ACM Trans. Graph.* 34, 4.
- STURM, J. 1999. Using SeDuMi 1.02, a MATLAB toolbox for optimization over symmetric cones. *Optimization Methods and Software* 11–12, 625–653. Version 1.05 available from <http://fewcal.kub.nl/sturm>.
- TAN, H. Z., PANG, X. D., AND DURLACH, N. I. 1992. Manual resolution of length, force, and compliance. *Advances in Robotics* 42, 13–18.
- TAN, H. Z., DURLACH, N. I., SHAO, Y., AND WEI, M. 1993. Manual resolution of compliance when work and force cues are minimized. *ASME Dyn. Syst. Control Div. Publ. DSC*, ASME, NEW YORK, NY,(USA), 1993, 49, 99–104.
- TIEST, W. M. B., AND KAPPERS, A. M. 2009. Cues for haptic perception of compliance. *Haptics, IEEE Transactions on* 2, 4, 189–199.
- WILLS, J., AGARWAL, S., KRIEGLAN, D., AND BELONGIE, S. 2009. Toward a perceptual space for gloss. *ACM Transactions on Graphics* 28, 4, 1–15.
- WU, W.-C., BASDOGAN, C., AND SRINIVASAN, M. A. 1999. Visual, haptic, and bimodal perception of size and stiffness in virtual environments. *ASME Dyn. Syst. Control Div. Publ. DSC* 67, 19–26.
- ZHANG, X., LE, X., PANOTOPOULOU, A., WHITING, E., AND WANG, C. C. L. 2015. Perceptual models of preference in 3D printing direction. *ACM Trans. Graph.* 34, 6 (Oct.), 215:1–215:12.